

In vivo and *in situ* evaluation of a wireless magnetoelastic sensor array for plastic biliary stent monitoring

Scott R. Green · Richard S. Kwon · Grace H. Elta ·
Yogesh B. Gianchandani

Published online: 5 March 2013
© Springer Science+Business Media New York 2013

Abstract This paper presents the *in vivo* and *in situ* evaluation of a system that wirelessly monitors the accumulation of biliary sludge in a plastic biliary stent. The sensing element, located within the stent, is a passive array of magnetoelastic resonators that is queried by a wireless electromagnetic signal. The *in vivo* and *in situ* testing uses commercially-available plastic biliary stents, each enhanced with an array of ribbon sensors (formed from Metglas™ 2826 MB). The sensor array is approximately 70 mm long and contains individual resonators that are 1 mm in width and have lengths of 10 mm, 14 mm, and 20 mm. The array is anchored into the 2.8 mm inner-diameter stent using a thermal staking technique. For the *in situ* testing, an instrumented stent is placed in various locations within the abdominal cavity of a female domestic swine carcass to evaluate the wireless range of the system; these results show that a wireless signal can be obtained from a range of at least 7.5 cm from a sensor array covered in bile. The *in vivo* testing includes the endoscopic implantation of an instrumented stent into the bile duct of a swine. After implantation, the swine was housed for a period of 4 weeks, during which the animal showed no ill effects and followed the expected growth curve from 29 kg to 42 kg. At the conclusion of the *in vivo* test, the animal was euthanized, and the instrumented stent explanted and examined. The results presented in this paper indicate that the monitoring system does not adversely affect the health of the animal and can feasibly provide sufficient wireless range after implantation.

Keywords Implant · Resonant Sensors · Biliary Sludge · Mass Sensors · Viscosity Sensors

1 Introduction

Stents are tubular structures used to establish and maintain patency within passages of the gastrointestinal tract that have become obstructed as a result of benign or malignant pathology. Though the act of placing a stent often relieves acute symptoms caused by the obstruction, stents are also at risk for obstruction due to accumulation of luminal contents, such as tissue or other biological matter.

An example of a stent application area—and the focus of this work—is the bile duct. Both metal self-expanding stents and plastic stents are used to treat biliary obstructions; however, the use of plastic stents is much more prevalent, especially in initial benign cases or as a means for reconstituting flow through a clogged metal stent [Classen et al. 2002; Libby and Leung 1996; Frattaroli et al. 1996; Kozarek 2000; McLean and Burke 1989; Somogyi et al. 2006; Davids et al. 1992]. Plastic stents range from 3 Fr to 11.5 Fr (1 mm to 3.6 mm) in diameter, with 10 and 11.5 Fr (3.2 mm and 3.6 mm) being the most commonly used in the bile duct. For plastic stents, which are typically used to palliate benign biliary obstructions, stent malfunction occurs frequently over an unpredictable timeframe of 1–6 months after implantation. The primary malfunction is formation of a bacterial matrix on and around the stent known as biliary “sludge” [Donelli et al. 2007; Sung 1995]. The sludge accumulates and eventually occludes the stent. Stent occlusion puts the patient at high risk for cholangitis (infection of the bile duct), which can lead to liver damage, sepsis, and death.

Current medical practice for diagnosis of a biliary obstruction—including an occluded stent—begins with the

S. R. Green (✉) · Y. B. Gianchandani
Center for Wireless Integrated MicroSensing and Systems
(WIMS2), Ann Arbor, MI, USA
e-mail: greensr@umich.edu

R. S. Kwon · G. H. Elta
Department of Internal Medicine - Gastroenterology,
University of Michigan, Ann Arbor, MI, USA

measurement of serum concentration of liver enzymes such as bilirubin and alkaline phosphatase, among others. Unfortunately, enzyme levels may not rise until after the blockage is significant, resulting in delayed intervention. Alternatively, endoscopic retrograde cholangiography can be performed to image the duct and diagnose a blockage, but this specialized endoscopic procedure is invasive and has a risk of complications and therefore is generally reserved only for therapeutic purposes—e.g., replacement of a stent that may be occluded. A direct, non-invasive method of diagnosis would enable timely intervention and prevent serious infectious complications.

The method outlined in Fig. 1 highlights an integrated system providing just such a direct, non-invasive measurement of sludge accumulation in a plastic biliary stent. The implanted device is a tubular plastic stent with an integrated array of magnetoelastic sensors. The sensor array is integrated along the inner sidewall of the stent to maintain an open flow channel and is queried remotely by a wireless radio frequency signal. In this design, there are three resonating sensors in the array, at different locations along the length of the stent, and each can be independently interrogated with a signal in an appropriate frequency band. External to the patient, circuitry drives wire coils to produce the interrogating magnetic field. The magnetic field causes the selected magnetoelastic sensor to resonate with a response which changes as local viscosity increases and as sludge accumulates. The response of the sensor is correlated to the local sensor environment—for example, the resonant frequency and quality factor can be used to measure the accumulated mass and bile viscosity.

We have previously reported on the basic architecture and bench-top performance of this system, as well as the performance of a single sensor in a self-expanding metal stent in *in situ* tests on a porcine carcass in a surgical setting [Green and Gianchandani 2009; Green et al. 2010; Green and Gianchandani 2010]. However, a number of key challenges remain regarding the feasibility of this technology in a practical clinical setting and utilizing an array of sensors.

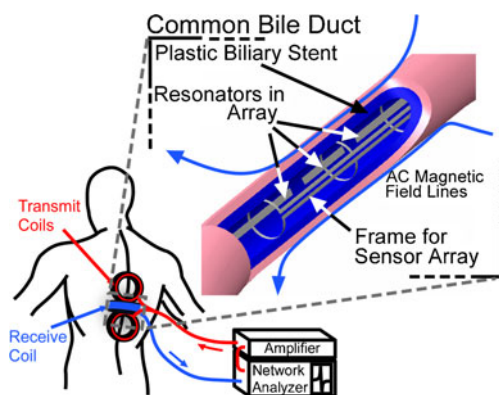


Fig. 1 Conceptual diagram of the magnetoelastic monitoring system

This work is directed at addressing these challenges, including sensor design; sensor-to-stent integration; interrogation module improvement for use in clinical settings; biocompatibility of key materials; and *in situ* and *in vivo* testing of the system. The focus of this work is the *in vivo* testing of a plastic biliary stent instrumented with a sensor array and the associated interrogation module; the design, fabrication, and *in situ* testing of the sensor and system are also described as part of this project leading up to the *in vivo* testing.

The design of the sensor array is presented in section 2. Also described in section 2 is the new interrogation approach that reduces background signal in the surgical and clinical environment. The fabrication of the sensor arrays and the process for integration of the arrays with the stents is discussed in section 3. Experimental methods and results for the *in vivo* and *in situ* testing are provided in section 4. The implications of the results are discussed in section 5, and the conclusions that can be drawn from this work are stated in section 6.

2 Design

2.1 Biliary stent

This work utilizes commonly used commercially available plastic (polyethylene) stents manufactured by Cook Endoscopy (Winston-Salem, NC; Cotton-Leung™ Biliary Stent). The stents have an outer diameter of 10 Fr (3.2 mm), an inner diameter of 2.8 mm, and an overall length of 9 cm (Fig. 2). When the stent is implanted, the proximal end generally is placed into the common hepatic bile duct, just outside the liver, while the distal end remains distal to the sphincter of Oddi in the small intestine. The stents include two “flaps” near the ends that extend outward into the local

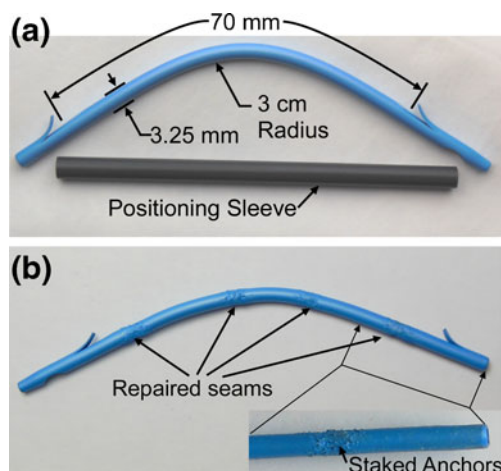


Fig. 2 **a** Plastic biliary stent, prior to sensor array integration. **b** Plastic biliary stent, with integrated sensor array. Inset: Thermally-staked sensor array anchors

anatomy and anchor the stent in the bile duct after placement. The stents also are fabricated with a longitudinal curvature of approximately 3 cm in radius; this is intended to better match the natural curvature of the bile duct.

The stent is placed in the desired implant location *via* an endoscopic procedure. The biliary orifice is first located endoscopically and then cannulated with a guide wire. Cannulation may be aided by an incision through the sphincter of Oddi, or biliary sphincterotomy. The stent is placed within a rigid plastic positioning sleeve, which straightens the stent, and then loaded onto an introducer assembly. The stent and introducer assembly are loaded onto the back end of the guide wire and advanced into the desired position. The introducer assembly pushes the stent out of the positioning sleeve so that the flaps can protrude and anchor the stent as designed.

For the purposes of this work, there are three main geometrical constraints on the design of the sensor array that are imposed by the plastic stent. The internal diameter of the stent is the first such constraint; the sensor array must fit within this diameter and remain close to the sidewall of the stent to ensure sufficient diameter for fluid flow. The second constraint is the length of the stent; the array must not be longer than the overall stent and ideally should fit between the flaps of the stent, where sludge is most likely to cause a flow blockage. The final constraint is the longitudinal curvature of the stent. The sensor and sensor array must conform to and accommodate this curvature. The thermo-plastic nature of the polyethylene stent allows features of the sensor array to be melted into the stent with local application of sufficient heat, although at the risk of diminishing sensor signal because of anchor losses. The evaluation and assessment of these constraints and risks are described in further detail in the fabrication and experimental results sections.

2.2 Magnetoelastic sensor array

Magnetoelastic transduction is a term used to describe the coupling between the classical properties of stress and strain and the quantum phenomenon of magnetism [Engdahl 2000]. Magnetoelastic behavior is most prominent in materials with strong coupling between the magnetic moment direction and the orientation of the elongated (anisotropically shaped) atom. Under an applied magnetic field, the coupled moments and atoms tend to rotate and align with the field, so that the magnetization and strain of the material is affected. From a macroscopic perspective, magnetoelastic coupling describes how the magnetization response to a magnetic field is related to the strain. For magnetoelastic materials used as resonant sensors, a simplified but useful understanding of the phenomenon would result from viewing the sensor as an oscillating dipole magnet, with the oscillations driven by the interrogative magnetic field. The

oscillating magnetic flux developed in the sensor can then induce a voltage on a suitably located antenna or pick-up coil. Changes in resonance characteristics, such as resonant frequencies and quality factors, are used to determine mass loading and viscosity [Green and Gianchandani 2010]. Changes in mass loading and viscosity can be interpreted by the physician as indicative of the progress of sludge accumulation and stent blockage.

An important aspect of stent monitoring is the ability to monitor the entire length of the stent for blockage. While this ability could be potentially provided by a single, very long sensor, there are two main drawbacks to that approach. First, the stent is subject to longitudinal curvature, and a long sensor would also experience such curvature. This curvature will tend to reduce the efficiency of the resonant vibrations of the sensor due to induced stress and geometrical changes, significantly diminishing signal amplitude and wireless range. Second, the response of a long sensor will be an averaged response to non-uniform sludge accumulation, diminishing sensitivity to critical levels of localized blockage. A superior option is an array of shorter sensors, each capable of being independently interrogated. The shorter sensors are less affected by stent curvature, and each sensor is sensitive only to sludge accumulation on and around that sensor.

For simplicity, a three-sensor array of 1 mm wide \times 25 μ m thick magnetoelastic ribbon-shaped sensors is chosen for this investigation (Fig. 3). To ensure that each sensor can be independently interrogated, the dimensions of each sensor are chosen such that the resonant frequencies of each are sufficiently separated. For example, the length dependence of the unloaded resonant frequency of a ribbon-shaped sensor, suspended at mid-length, is described by the well-known equation

$$f_n = \frac{1}{L_n} \sqrt{\frac{E}{\rho}}, \quad (1)$$

where f_n is the resonant frequency of the n th sensor, L_n is the length of the n th sensor, E is the Young's Modulus of the

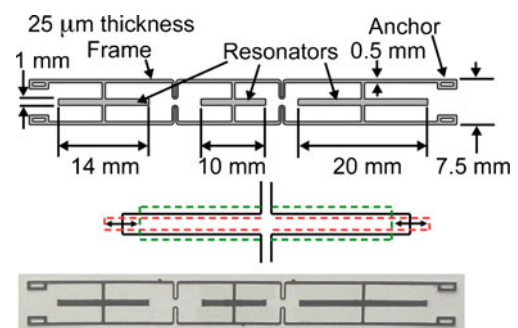


Fig. 3 **a** Sensor array layout and important dimensions. **b** Deformed shape of the longitudinal vibrational mode stimulated in the resonators during interrogation. **c** Fabricated sensor array

sensor, and ρ is the mass density of the sensor. For this application, at a full load, the unloaded resonant frequencies are expected to decrease by 10 %, and the bandwidth of the resonant peak is expected to grow from 1 % to approximately 30 % of the center frequency. These specifications are based on our previous experience with similar sensors. These specifications, in conjunction with Eq. (1), are used to select the length of each sensor such that the loaded response will not overlap with the response of the other sensors in the array. For the ribbon array and the chosen lengths of 10 mm, 14 mm, and 20 mm, the expected resonant frequencies are 206 kHz, 147 kHz, and 103 kHz, respectively. The resonant response of unloaded sensors in this array can also be estimated using the magnetomechanical finite element analysis method described in [Green and Gianchandani 2009].

In each array, the resonators are connected with a frame. This frame has u-shaped features between each resonator, which are intended to reduce the longitudinal stiffness of the frame to better accommodate the stent curvature in this direction. Like the resonators, the frame is designed to nest closely with the inner sidewall of the stent. At the ends of the frame are anchors. These anchors are to be melted into the stent, using the thermal staking process described in the fabrication section.

2.3 Interrogation module

The interrogation module refers to all of the external (i.e. not implanted) components that are required to send and receive alternating magnetic field information to and from the sensor. There are four main components of the interrogation module: a network analyzer, an amplifier, transmit coil(s), and receive coil(s). The coils are configured such that the transmit coils and receive coils can both couple to the sensor, but not with each other (Fig. 4). The interrogative field lines emanate from one transmit coil, loop through the sensor position such that the field lines are longitudinally aligned with the sensor, and terminate in the other transmit coil. The response field lines emanate from the sensor and are in essentially the same pattern as they would be if emanating from a dipole magnet. Thus, the receive coils are located at null points of the transmitted signal (i.e. are oriented perpendicular to the direction of the transmit field), yet are aligned with the resulting field from the sensor. This arrangement helps to decouple the transmit signal from the received signal, improving the signal-to-noise ratio. Important dimensions of the coil configuration are listed in Table 1.

For this work, the coils have been turned using 60-stranded 22 AWG Litz wire, in which each individual conducting strand is insulated. For oscillating currents at the higher frequencies used in this work, the skin effect in a

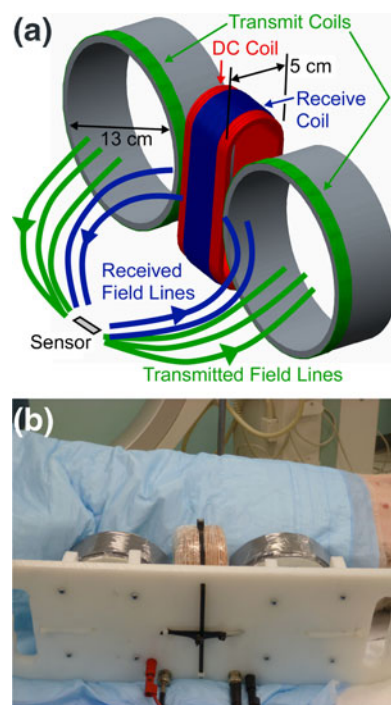


Fig. 4 a Schematic of the interrogation coils used in this work. b Orientation of coils with respect to animal during interrogation

conductor is important in determining the overall impedance of the conductor. The individually-insulated conductors in the Litz wire are meant to reduce the skin effect and provide a higher conductance for high frequency signals. The higher conductance results in lower noise in the voltages induced on the receive coil, serving to increase the wireless range of the system. Similarly, the number of turns in the transmit coils have been reduced in order to lower the coil impedance and increase the magnitude of the transmitted magnetic field at the frequencies of interest. Overall, these changes increase the SNR by a factor of 7 compared to our previous work [Green et al. 2010].

Table 1 Coil configuration dimensions and performance

Transmit Coil Diameter (cm)	13
Transmit Coil # of Turns (each)	10
Transmit Coil Length (cm)	1.8
Transmit Coil Wire Type	22 AWG Litz (60 strands)
Receive Coil Dimensions (cm)	5 wide × 13 tall
Receive Coil # of Turns	32
Receive Coil Wire Type	22 AWG Litz (60 strands)
DC Coil Dimensions (cm)	5 wide × 13 tall
DC Coil # of Turns	90
DC Coil Wire Type	16 AWG speaker wire
SNR for Unloaded 5 mm × 18 mm 2826 MB Ribbon Sensor (5 cm from extracorporeal setup)	70

This effort sought to enhance the interrogation module by automating a differential method for canceling the baseline shifts (common mode coupling shifts) that occur in a surgical environment. Experimental characterization efforts have shown that conductive materials in the surgical or clinical setup near the interrogation coils can shift the baseline measurement and obscure the sensor signal. To combat this issue, this work implements a controllable electromagnet in the interrogation coils, along with a method for continuously sampling and canceling the baseline while the coils are in the measurement location.

In the manifestation used in this work, the controllable electromagnet is formed from 16 AWG speaker wire, and consists of 90 turns (6 layers of 15 turns each) layered under the receive coil. The resistance of the electromagnet coil is nominally 2.5Ω . When provided with 1 A of DC current, this coil generates a horizontal magnetic field of approximately 1.5 Oe at 5 cm and 0.5 Oe at 11 cm from the interrogation coils.

The interrogation method is described in Fig. 5. In this method, the baseline is taken while the coils are in position but the sensor is turned “off” by not applying a DC bias field. Then, the sensor can be turned “on” by applying the DC bias field *via* the electromagnet. The baseline signal can then be subtracted from the active signal. This process can be done in a loop while averaging consecutive sweeps together to further reduce the signal noise. For this work, this method is implemented using a LabView (National Instruments; Austin, Texas, USA) program, along with a B&K Precision 1696 DC power supply *via* a serial (RS-232) connection and a GPIB connection for the Agilent 4395A network analyzer.

3 Fabrication

3.1 Sensor arrays

As previously noted, the arrays consist of the individual sensors, linked together in a frame with anchoring features at

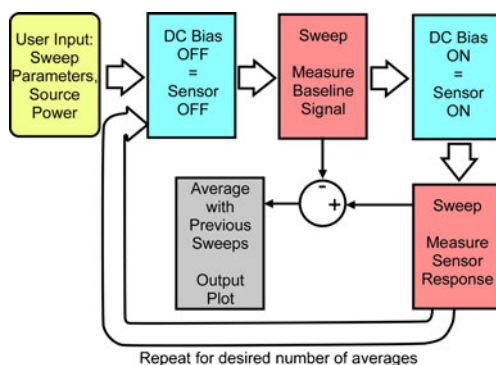


Fig. 5 Flow chart illustrating the interrogation protocol for canceling background signals

each end. The sensor arrays are fabricated, in a planar state, from Metglas™ 2826 MB (a nickel-iron-molybdenum-boron alloy) using the photochemical machining process (Fig. 10) [ASM Handbook 1989]. In order to nest closely with the inner sidewall of the stent, the array is given a lateral curvature by using a thermal annealing process (Fig. 6). The arrays are placed on a thin aluminum foil, and held on the foil with a 1.5 mm diameter brass rod. The foil and array are then wrapped tightly around the rod, with the aluminum foil holding the shape of the rod and thus causing the array within to also hold the same shape. While held in this fixture, the assembly is placed in a vacuum oven and exposed to a temperature of 275 °C for 12 h at a vacuum level of 30 mTorr. The Metglas™ alloy from which the sensor array is made contains iron and tends to corrode in air at high temperatures; the vacuum level used here reduces corrosion during the process to a negligible level. Although a higher temperature can shorten the required annealing time, it also will tend to embrittle the array material. Temperatures exceeding the crystallization temperature (430 °C for this alloy) should also be avoided in order to retain the magnetostrictive properties of the foil. The annealing process used in this work results in an array and frame with a lateral radius of curvature of approximately 1.5 mm. After the annealing process, the sensor arrays are coated conformally with a 2 μm thick layer of Parylene C, which minimizes post-implant corrosion of the sensor array and enhances biocompatibility.

3.2 Integration of sensor arrays and biliary stents

The sensor arrays and biliary stents are integrated using a thermal staking method. The polyethylene stent is slit manually with a razor blade at four locations coinciding with the anchors of the sensor array frame and the two portions of the frame between the individual resonators. The intermediate slits assist in threading the array into the stent. Once the array has been threaded through the stent segments, the intermediate slits are repaired using local heat from a soldering iron (175 °C) and manually applied compression. This action causes the polyethylene of the stent to melt and inter-diffuse across the slit. To join the array with the stent, the anchors in the frame of the array are used. The anchors extend beyond the remaining slits in the stent, and

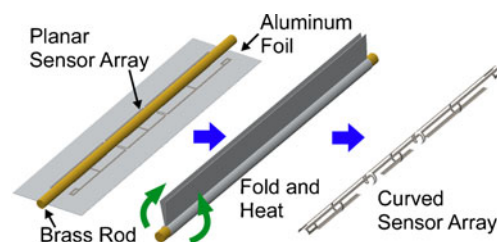


Fig. 6 Process flow for adding lateral curvature to sensor arrays

during the repair of these slits are kept on the outer surface of the stent. After repairing the slits, the anchors are staked into the outer surface of the stent again using the local soldering iron heat and manually applied pressure. Figure 2 shows an example of an instrumented stent. In the long term, the polyethylene stents can be molded in place around the sensor array frame.

4 Experimental methods and results

4.1 Benchtop assessment of arrays

The sensor arrays were tested after photochemical machining, after addition of transverse curvature, and after integration with stents to evaluate the effect on measurable signal of each of these steps. After photochemical machining and before any other processes, the typical measured signal and resonant frequency from the arrays at a distance of 5 cm is as listed in Table 2.

After going through the lateral curvature process, measured resonant frequencies were typically shifted upwards significantly by about 50 %. The measured amplitudes were not significantly affected. Integration with the stent did not introduce any further significant changes.

4.2 Cytotoxicity testing

The magnetoelastic materials used in this work represent a relatively new and relatively untested class of candidates for use in medical implants. According to the Food and Drug Administration guidance detailed in ISO 10993 and Blue Book Memorandum G95-1, the first step in full biocompatibility testing for a chronically implanted medical device includes evaluating potential for cytotoxicity. In this case, our goal was to evaluate the magnetoelastic material (Metglas™ 2826 MB) in its as-cast condition, rather than after further processing or as part of a medical device. As such, material was provided to Toxikon (Bedford, MA, USA), a leading provider of certified biocompatibility testing, for a standard cytotoxicity test. The samples (75 cm² in area) were provided in a non-sterile condition, and were exposed to a United States Pharmacopeia

(USP) standard Minimum Essential Medium (MEM) elution test. The results of this test indicate that the base material shows considerable signs of cytotoxicity. For this reason, the sensor arrays used with *in situ* and *in vivo* testing have been coated with Parylene C, which is a material often used to protect biomedical implants and is considered biocompatible [Stark 1996]. Future work should further address biocompatibility of the sensor material and any coatings.

4.3 *In situ* testing

For *in situ* testing of the sensor array, a procedure similar to that used and discussed in [Green et al. 2010] was used. After euthanization of a female domestic swine of approximately 42 kg mass, a laparotomy was performed. Throughout the test, the animal was positioned on its dorsal surface. The bile duct was located visually, and a duodenostomy was performed in order to access the duct. Under direct visualization, the device (integrated stent and sensor array) was deployed into target locations without using the positioning sleeve. Prior to deployment, the instrumented stent was filled with bile from the bile duct. In sequential tests, the instrumented stent was positioned first against the ribcage of the animal, then between the lobes of the liver at a location approximately 7.5 cm from the external surface of the animal, and then in the bile duct (approximately 11 cm from the external surface of the animal). In each case, the long axis of the stent was oriented generally along the long axis of the animal. After placing the instrumented stent, the interrogation coils were placed against the external lateral surface of the animal, generally parallel with and centered on the instrumented stent (Fig. 4). The interrogation module was then used to query each sensor in the array, with the procedure described in section IC. The DC magnetic field applied to each sensor as a bias was approximately 4 Oe.

Figure 7 shows the measured response of the 20-mm-long resonator when located at a distance of 7.5 cm from the external surface of the animal, with the instrumented stent filled with bile and placed between the lobes of the liver. The resonant frequency is approximately 114 kHz, and the signal-to-noise ratio is a robust 30. Figure 8 shows the measured response of the 14-mm-long resonator when located at a distance of 7.5 cm from the external surface of the animal, with the instrumented stent filled with bile and placed between the lobes of the liver. The resonant frequency is approximately 165.3 kHz, and the signal-to-noise ratio is 10. No signal could be observed from the 10-mm-long resonator in this position, and no signal could be observed from any resonator when the stent was placed 11 cm from the surface of the animal in the bile duct.

Table 2 As-cast resonator performance

(5 cm wireless range)	Resonant Frequency (kHz)	Signal Amplitude (μ V)
20 mm Resonator	71	155
14 mm Resonator	110.7	50
10 mm Resonator	132.5	75

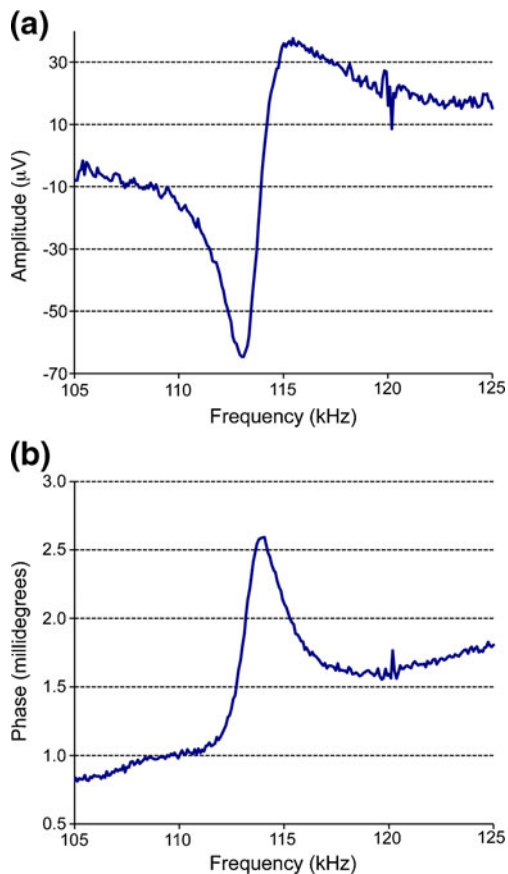


Fig. 7 Measured magnitude (a) and phase (b) response of the 20 mm long ribbon resonator. The interrogation distance is 7.5 cm, and the instrumented stent is full of bile and located in between lobes of the liver

4.4 *In vivo* testing

The *in vivo* testing was carried out with an Institutional Review Board approved protocol, #10330-1 in the University of Michigan system. The animal for this test was a female domestic swine. The initial weight of the animal was 29 kg. The chest and abdominal region of the animal was initially approximately 22 cm in diameter. Prior to the implantation procedure, a stent instrumented with a sensor array was sterilized using a steam autoclaving process. An Olympus side-viewing duodenoscope was sterilized prior to the procedure using a standard ethylene oxide sterilization process. The instrumented plastic biliary stent was mounted on a delivery system intended for use with the stent consisting of a wire guide, pushing catheter, and guiding catheter (Cook Endoscopy, Winston-Salem, NC).

The stent was deployed endoscopically into the bile duct of the animal in standard endoscopic fashion. After intubation of the animal and induction of general anesthesia, the duodenoscope was passed orally into the upper gastrointestinal tract and specifically to the ampullary orifice (bile duct opening). Using the catheters and guidewires, the common

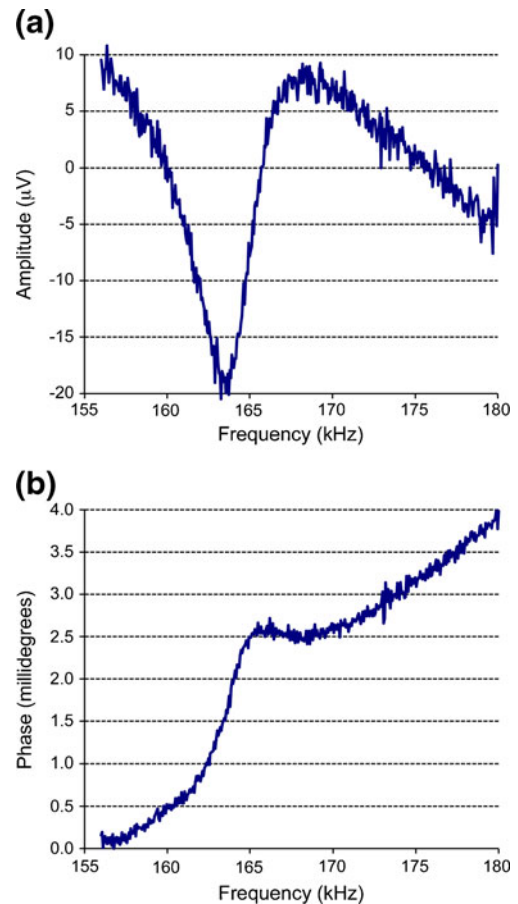


Fig. 8 Measured magnitude (a) and phase (b) response of the 14 mm long ribbon resonator. The interrogation distance is 7.5 cm, and the instrumented stent is full of bile and located in between lobes of the liver

bile duct was cannulated under fluoroscopic guidance. An initial cholangiogram was performed to delineate the anatomy. The stent was then deployed into the bile duct over the guidewire under fluoroscopic guidance. After proper stent position was confirmed (Figs. 9 and 10), the scope was removed from the animal. The final position of the stent was approximately aligned on the long axis of the animal (11 cm from the surface of the animal) and aligned with the posterior extent of the ribcage.

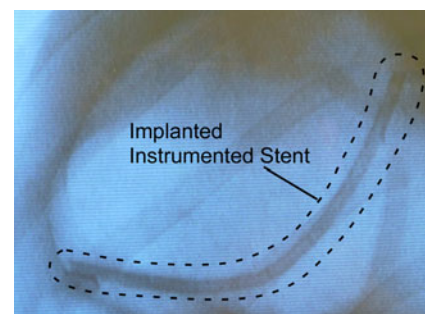


Fig. 9 Fluoroscopic image of implanted stent

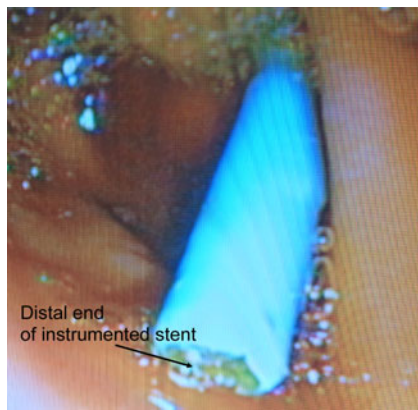


Fig. 10 Endoscopic image of implanted stent, showing protrusion of the distal end into the duodenal space

After the initial stent placement, the sensor array was interrogated using the same method as described in section 4.3. Following this, the animal was recovered in the post-operative facilities before being transferred to standard animal housing. For the next month, the animal was housed and monitored twice daily for any signs of sickness, including fever, lethargy, loss of appetite, and loose stool. Throughout this period, the animal remained bright, alert, and responsive with normal heart and respiration rates and normal body temperature. A blood test was taken after 2 weeks with results in the normal range for the animal. The animal put on weight at a normal rate, and by the end of this period weighed approximately 42 kg.

During the month of housing and monitoring, the animal was anesthetized once a week for further attempts at interrogating the sensor array. During these sessions, the pig was sedated, then intubated and anesthetized for approximately 2 h. As was the case during the initial interrogation session immediately after implant, no signal was measured in any of these sessions.

After the final recording attempt at the end of the survival month, the animal was euthanized with an overdose of barbiturates per standard protocol and the instrumented stent was harvested and inspected visually (Fig. 11). The stent was found to have been positioned approximately 11 cm from the surface of the animal. The stent was filled with bile upon harvesting; no evidence of sludge build up was present. The distal (duodenal) end of the stent had broken off, with the failure point coinciding with one of the re-melted seams. The stent was cut apart to inspect the sensor array. Although the anchors and portions of the frame remained intact, it was found that the resonators had been damaged and portions were missing.

5 Discussion

Though the *in vivo* testing showed that the presence of the instrumented stent did not cause health problems over the



Fig. 11 Post-necropsy image of distal (duodenal) end of stent

course of the month of survival, it also illuminated some challenges with the sensor packaging that still must be addressed. First, the repaired seams that result from the thermal staking process were shown to be a weak point. This is especially the case when placed under lateral mechanical loading, as occurred in this work. It is believed that the exposure of the distal end of the stent to the digestive matter passing through the duodenum, along with the weakness of the repaired seam, resulted in the breakage shown in this work. The second packaging issue that must be addressed is the protection of the resonators while mounting on the delivery assembly and during implantation. It is believed that the act of passing the instrumented stent over the introducer during implantation resulted in this damage. Given the success of the post-euthanization *in situ* tests described in section 4.3, it appears evident that the absence of unharmed resonators was the main factor for being unable to acquire a signal from the implanted array in the *in vivo* tests.

6 Conclusion

The goal of the proposed work was to enhance the options available for monitoring stent occlusion by developing and validating a wireless system that measures mass and viscosity changes caused by adherent occlusive material. The key component of this system is a magnetoelastic resonant sensor array integrated with a plastic biliary stent.

Sensor design focused on arraying of frequency-distinct segments, providing the ability to determine the axial position of the buildup. Another focus was the facilitation of integration of the sensor with the stent. In this design iteration, anchors and linkages were incorporated. The thermo-plastic nature of the polyethylene stents was used to heat-stake the anchors into the stent.

Biocompatibility tests, starting with cytotoxicity testing of the base material, were completed. These studies have

confirmed the need for coating materials. The sensors were coated with 2 μm of Parylene-C to provide a biocompatible protective coating.

Custom electromagnetic coils, used for interrogating the sensors while minimizing background noise, were designed. These coils were fabricated in a setup targeted for *in vivo* testing and controlled with a custom computer-automated system for “chopping” the sensor interrogation to cancel background noise.

Fabricated sensors were integrated with stents and evaluated by *in situ* testing. This testing showed improved signal range of at least 7.5 cm within the swine carcass, with sensors positioned in the proximity of the liver. *In vivo* testing on a swine was also conducted. The instrumented stent was implanted using an endoscopic approach. Over the course of 4 weeks, the swine was monitored daily for health. A blood sample was drawn midway through the testing. The swine remained healthy throughout the test, including a normal weight gain from a starting weight of 29 kg to a final weight of approximately 42 kg. No signal was measured from the implanted array; this was attributed to damage to portions of the sensor array that occurred during implantation. Future work should focus on the improvement of the robustness of the sensor-array-to-stent integration process and the protection of the sensor array during implantation.

Acknowledgements Metglas Inc. provided samples for this project. The authors gratefully acknowledge Gail Rising, Amber Yovanovich, and Dr. Srinivas Chiravuri, who provided intubation and anesthesia administration expertise during the *in vivo* testing. This work was supported by the National Institutes of Health and the University of Michigan.

References

- M. Classen, G. Tytgat, C. Lightdale, *Gastroenterological Endoscopy*, Thieme, (2002)
- P. Davids, A. Groen, E. Rauws, G. Tytgat, K. Huibregtse, Randomised trial of self-expanding metal stents versus polyethylene stents for distal malignant biliary obstruction. *Lancet* **340**(Dec. 19-26), 1488–1492 (1992)
- G. Donelli, E. Guaglianone, R. Di Rosa, F. Fiocca, A. Basoli, Plastic biliary stent occlusion: factors involved and possible preventive approaches. *Clin. Med. Res.* **5**(1), 53–60 (2007)
- G. Engdahl (ed.), *Handbook of Giant Magnetostrictive Materials* (Academic, London, 2000), pp. 1–19
- F. Frattaroli, D. Reggio, A. Guadalaxara, Benign biliary strictures: a review of 21 years of experience. *J. Am. Coll. Surg.* **183**(5), 506–513 (1996)
- S. Green, Y.B. Gianchandani, Wireless magnetoelastic monitoring of biliary stents. *J. Microelectromech. Syst.* **18**(1), 64–78 (2009)
- S. Green, R. Kwon, G. Elta, Y.B. Gianchandani, In situ and Ex vivo evaluation of a wireless magnetoelastic biliary stent monitoring system. *Biomed. Microdevices* **12**(3), 477–484 (2010)
- S. Green, Y.B. Gianchandani, Tailored Magnetoelastic Sensor Geometry for Advanced Functionality in Wireless Biliary Stent Monitoring Systems. *J. of Micromech. and Microeng.*, (2010) ASM Handbook, Vol. 16, ASM International, (1989)
- R. Kozarek, Metallic biliary stents for malignant obstructive jaundice: a review. *World J. Gastroenterol.* **6**(5), 643–646 (2000)
- E. Libby, J. Leung, Prevention of biliary stent clogging: a clinical review. *Am. J. Gastroenterol* **91**(7), 1301–1307 (1996)
- G. McLean, D. Burke, Role of endoprotheses in the management of malignant biliary obstruction. *Radiology* **170**, 961–967 (1989)
- L. Somogyi, R. Chuttani, J. Croffie, J. DiSario, J. Liu, D. Mishkin, R. Shah, W. Tierney, L. Wong Kee Song, B. Petersen, Biliary and pancreatic stents. *Gastrointest. Endosc.* **63**(7), 910–919 (2006)
- N. Stark, Literature review: biological safety of Parylene C. *Med. Plast. Biomater.* **3**(2), 30–35 (1996)
- J. Sung, Bacterial biofilm and clogging of biliary stents. *J. Ind. Microbiol.* **15**, 152–155 (1995)